NANO LETTERS

Letter

pubs.acs.org/NanoLett

Metal–Insulator–Semiconductor Nanowire Network Solar Cells

Sebastian Z. Oener,[†] Jorik van de Groep,[†] Bart Macco,[‡] Paula C. P. Bronsveld,[§] W. M. M. Kessels,[‡] Albert Polman,[†] and Erik C. Garnett*[,†]

[†]Center for Nanophotonics, FOM Institute AMOLF, Science Park 104, 1098 XG, Amsterdam, The Netherlands

[‡]Department of Applied Physics, Eindhoven University of Technology, 5600MB Eindhoven, The Netherlands

[§]ECN Solar Energy, Westerduinweg 3, 1755ZG Petten, The Netherlands

Supporting Information

ABSTRACT: Metal–insulator–semiconductor (MIS) junctions provide the charge separating properties of Schottky junctions while circumventing the direct and detrimental contact of the metal with the semiconductor. A passivating and tunnel dielectric is used as a separation layer to reduce carrier recombination and remove Fermi level pinning. When applied to solar cells, these junctions result in two main advantages over traditional p–n-junction solar cells: a highly simplified fabrication process and excellent passivation properties and hence high open-circuit voltages. However, one major drawback of metal–insulator-semiconductor solar cells is that a continuous metal layer is needed to form a junction at the surface of the silicon, which decreases the optical transmittance and hence short-circuit current density. The decrease of transmittance with increasing metal coverage, however, can be overcome by nanoscale structures. Nanowire networks exhibit precisely the properties that are required for MIS solar cells: closely spaced and conductive metal wires to induce an inversion layer for homogeneous charge carrier extraction and simultaneously a high optical transparency. We experimentally demonstrate the nanowire MIS concept by using it to make silicon solar cells with a measured energy conversion efficiency of 7% (~11% after correction), an effective open-circuit voltage (V_{oc}) of 560 mV and estimated short-circuit current density (J_{sc}) of 33 mA/cm^2. Furthermore, we show that the metal nanowire network can serve additionally as an etch mask to pattern inverted nanopyramids, decreasing the reflectivity substantially from 36% to ~4%. Our extensive analysis points out a path toward nanowire based MIS solar cells that exhibit both high V_{oc} and J_{sc} values.

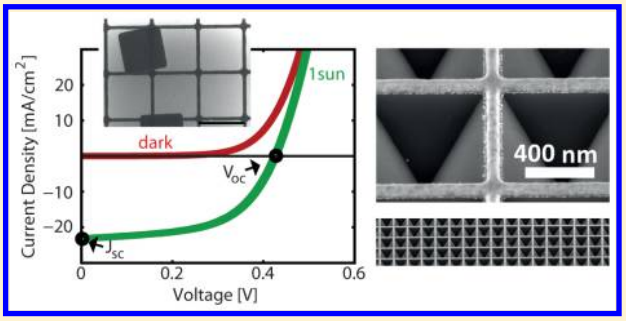

KEYWORDS: *Metal–insulator–semiconductor, solar cells, nanowire networks, nanopyramids*

When a metal contacts a semiconductor, a carrier selective Schottky junction can be formed. The resulting conduction type inversion in the semiconductor depends on the metal and semiconductor work function difference. For example, when n-type silicon directly contacts a high work function metal (Au), the conductivity for electrons falls below the conductivity for holes close to the surface. This inversion of the majority carrier conduction type causes the carrier selective properties of Schottky junctions. However, the direct contact between metal and semiconductor can increase surface recombination due to metal induced band gap states and dangling bonds and can even lead to Fermi level pinning at the semiconductor surface.[1] Metal–insulator–semiconductor (MIS) junctions circumvent those problems by separating the metal and semiconductor with a thin tunnel and passivating dielectric.[2] Furthermore, interface charges at the dielectric semiconductor interface can increase the magnitude of the conduction type inversion in the semiconductor.[3]

Because of their charge selective and passivating properties, MIS junctions were successfully used to make silicon solar cells starting in the 1970s.[4,5] The MIS solar cell device architecture has two main advantages over traditional p–n junction cells: (1) highly simplified fabrication and (2) excellent passivation of the semiconductor even under the contact.[4,6] For traditional solar cells, highly doped regions are required to induce the charge selectivity with the disadvantage of increased Auger recombination. The reduced carrier recombination of MIS solar cells led to open-circuit voltage (V_{oc}) values of up to 655 mV, surpassing those of traditional p–n junction solar cells in early development stages.[2] More recently, the extraordinary potential of the MIS concept has emerged again with recent record silicon solar cells employing a carrier selective, tunnel oxide passivated contact at the back side, which is conceptually identical to the MIS structure.[6−8] Furthermore, the MIS junction has emerged as one of the most successful interfaces in photocatalysis in recent years, where the metal induces charge separation, catalyzes the chemical reaction, and protects the underlying semiconductor.[9−12]

One major difficulty in applying MIS contacts to the front of a solar cell is the increased reflection due to the required metal

Received: March 4, 2016
Revised: April 14, 2016
Published: May 12, 2016

ACS Publications © 2016 American Chemical Society

DOI: 10.1021/acs.nanolett.6b00949
Nano Lett. 2016, 16, 3689–3695

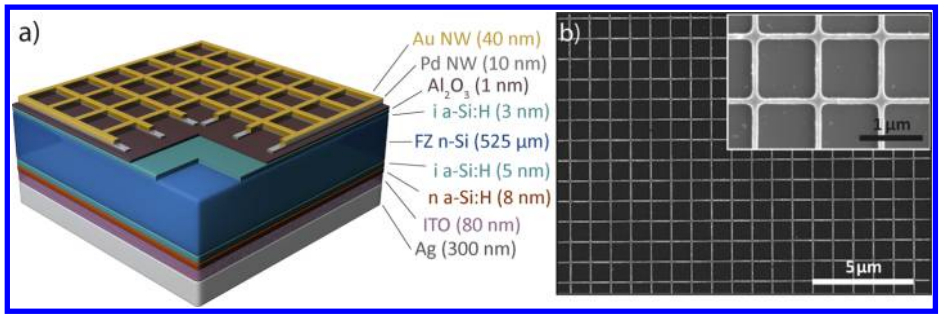

Figure 1. (a) Device schematic, showing the different layers employed for the nanowire network MIS solar cell. Not to scale. (b) SEM images of the nanowire network with 100 nm nanowire width, 50 nm height, and 1 μm pitch on top of the silicon half-cell, showing the high uniformity of the nanoscale pattern. A high-resolution SEM is shown as an inset.

coverage for homogeneous junction formation. Early generations of MIS solar cells utilized thin metal layers and hence exhibited low short-circuit current densities (J_{sc}), while advanced generations introduced widely spaced macroscopic contact fingers that reduced the reflection substantially and led to substantial performance improvements.[13] To form a homogeneous junction under the whole surface, additional dielectric layers with a high fixed charge density were employed, which however were insufficient to induce junction properties similar to diffused junctions or continuous metal layers.[13] Therefore, a low reflectivity combined with a high quality homogeneous MIS junction over the entire surface, which is especially needed for materials with short carrier diffusion lengths, remains to be a challenge for the MIS device architecture.

The decrease of transmittance with increasing metal coverage of homogeneous MIS junctions can be overcome by nanoscale structures. Even though their electrical performance approaches those of continuous thin-films, engineered metal nanowire networks have been demonstrated to exhibit extraordinary transmission, where the transmission is larger than expected from geometric considerations.[14−19] Furthermore, nanowire networks can be fabricated on a large scale with roll-to-roll compatible processes, like nanoimprint lithography, or even using solution-synthesized metal nanowires.[20−24] Therefore, nanowire networks exhibit precisely the properties that are required for MIS solar cells: closely spaced and conductive metal wires to induce a junction for homogeneous carrier extraction and, simultaneously, a high optical transparency.

Here, we demonstrate nanowire network based MIS silicon solar cells by fabricating the nanowire networks on top of passivated c-Si half cells using electron beam lithography. By choosing well-passivated silicon as a base material, we are able to exclude any effects of short minority carrier diffusion lengths on our results. Our solar cells exhibit a measured conversion efficiency of 7%. After correcting for the influence of the small size of the active area on the V_{oc} and the missing antireflection coating on the I_{sc}, we estimate that our MIS solar cells exhibit a corrected power conversion efficiency of ∼11% with an effective V_{oc} of 560 mV and estimated J_{sc} of 33 mA/cm^2. We perform electron-beam-induced current (EBIC) measurements to prove that nanowire networks can be used to form an MIS junction, which leads to homogeneous charge carrier extraction. Band diagram simulations allow us to investigate the dependence of the conduction type inversion on the work function difference between the metal and the semiconductor and hence to explain the relatively low V_{oc}. Reflection measurements show that a high metal coverage of the surface with metal nanowire networks only slightly increases reflection compared to a flat silicon surface. Finally, we demonstrate a first step toward improved device performance by using the metal nanowire network not only as a transparent electrode and for the inversion layer formation, but also as an etch mask for surface texturing. We fabricate inverted nanopyramids integrated into the metal nanowire network. As a result, we are able to decrease the reflectivity substantially from 36% to ∼4%. We use external quantum efficiency (EQE) measurements to estimate the influence of the reduced reflection on the overall device performance and thereby point out a path toward MIS solar cells that exhibit both high V_{oc} and J_{sc} values.

Fabrication. To isolate the effect of the metal nanowire network on the MIS solar cell performance, we use a state-of-the-art contact scheme for the back of the solar cell, which is employed in industrial silicon heterojunction (SHJ) solar cells (see Figure 1a and Methods). It consists of 5 nm of intrinsic a-Si:H followed by 8 nm of n-type a-Si:H, 80 nm ITO, and 300 nm Ag. Because of the importance of the tunnel and passivation layer, we rely on a high quality double layer for the front surface, consisting of 3 nm intrinsic hydrogenated amorphous silicon (a-Si:H), followed by 1 nm of Al_2O_3.[25] The intrinsic a-Si:H is grown by inductively coupled plasma chemical vapor deposition (ICP-CVD) and is used due to the excellent chemical passivation properties on the silicon surface. The Al_2O_3 layer is grown by atomic layer deposition (ALD) and is known for its high stability and insulating properties.[26] When used directly on silicon, ALD-Al_2O_3 has been shown to exhibit a high fixed charge density, which can lead to a field effect passivation of the underlying surface.[27−30] Besides the additional passivation effect, the Al_2O_3 also serves as a capping layer to prevent the out diffusion of hydrogen from the intrinsic a-Si:H layer. The metal nanowire network is fabricated by electron beam lithography on small areas (2.4−4.5 mm^2) and subsequent metal evaporation of Pd and Au. Pd was chosen due to the high work function to create a strong inversion layer, while Au was used because of lower optical losses than Pd. The low stability of Ag during subsequent processing precluded a possible usage of that metal. To integrate the inverted nanopyramid texturing in between the metal nanowire networks, the networks are fabricated on a silicon wafer, which is subsequently immersed in a KOH solution (further details in Methods section).

Results. Figure 1b shows the fabricated Au−Pd nanowire network on top of the passivated substrate. The wires are 100 nm wide, 50 nm high (10 nm Pd/40 nm Au), and the pitch is 1 μm. The network is highly uniform and spans an area of 2.4 mm^2.

DOI: 10.1021/acs.nanolett.6b00949
Nano Lett. 2016, 16, 3689−3695

Figure 2a shows the current density−voltage (J−V) traces of a masked nanowire network MIS solar cell under 1 sun illumination (green) and in the dark (red). The inset shows a schematic of the 2.4 mm^2 solar cell, which is created by fabricating a nanowire network (red) on top of a 2 cm^2 large substrate (blue). The silver back contact (gray), the contact probes (black) and the shadow mask (green) are indicated. The J−V curve in the dark shows a clear rectification. Under 1 sun illumination intensity, an open-circuit voltage (V_{oc}) of 423 mV, a short-circuit current density (J_{sc}) of 23 mA/cm^2, and a fill factor (FF) of 58% are obtained.

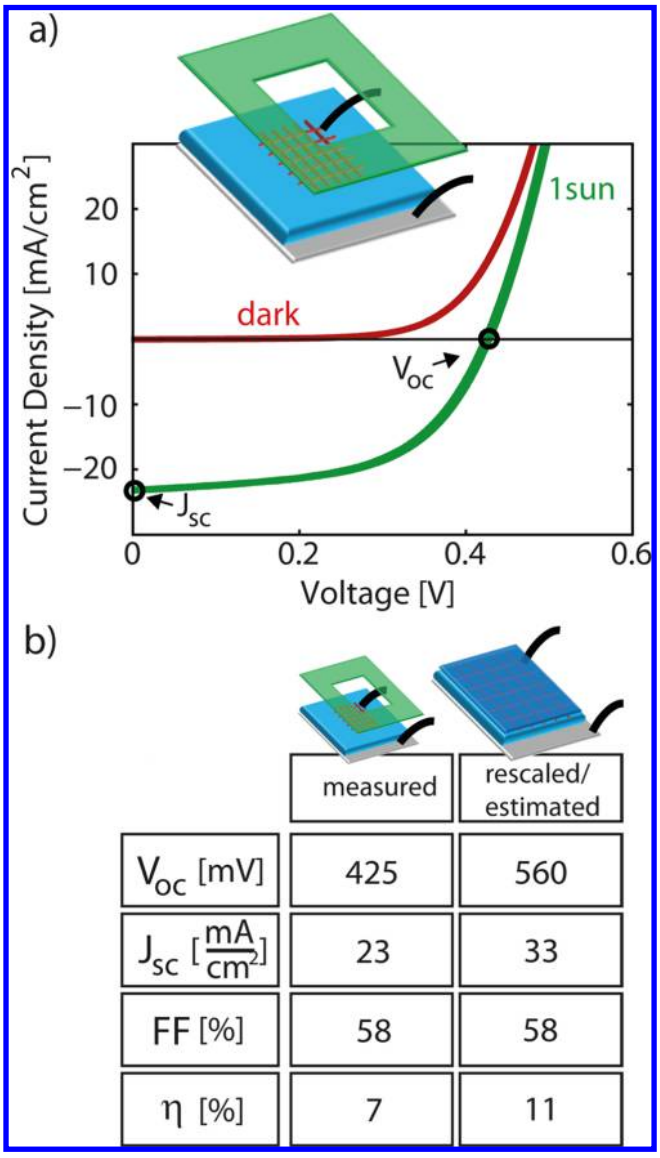

	measured	rescaled/ estimated
V_{oc} [mV]	425	560
J_{sc} [mA/cm^2]	23	33
FF [%]	58	58
η [%]	7	11

Figure 2. (a) J−V trace of nanowire network MIS solar cells in the dark (red) and under 1 sun (AM1.5G) illumination intensity (green). The active area shown here has a size of 2.4 mm^2 on a 2 cm^2 substrate. The measurements are performed under masked conditions. The inset shows the experimental geometry, where the nanowire network (red) and the shadow mask (green) are used to define the cell area. (b) Table with the measured and rescaled/estimated solar cell parameters.

To account for the smaller size of the masked collection area (2.4 mm^2) compared to the substrate area (2 cm^2) we calculate the impact on the V_{oc}, with the main effect being the high contribution of the recombination current (I_0) originating from a larger area than the I_{sc}. As explained in detail in the SI, we use two different approaches to estimate the effective V_{oc}, both resulting in the same value of about 560 mV (see Figure S1−5). Finally, we estimate the current density with an antireflection (AR) (n = 2) coating with 10% residual reflectivity (simulated value), compared to the uncoated solar cell (36% measured reflectivity). Figure 2b shows a table with the measured and rescaled/estimated solar cell parameters, taking into account the aforementioned effects. As a result, the nanowire network MIS solar cell has an effective V_{oc} of 560 mV, an estimated J_{sc} of 33 mA/cm^2 and a FF of 58%, resulting in an 11% energy conversion efficiency (after correction).

The results show that the metal nanowire network not only gives rise to charge carrier extraction but also charge carrier separation inside the semiconductor, that is, the metal nanowire network can potentially be used to replace the traditional contacts of an MIS solar cell. The small spacing of the metal networks makes our MIS concept applicable to materials with minority carrier diffusion lengths ∼1 μm, as is the case for many thin film materials such as CIGS, CdTe, halide perovskites and GaAs (see also Figure 3).[31] However, our results also show that our obtained solar cell parameters, that is,

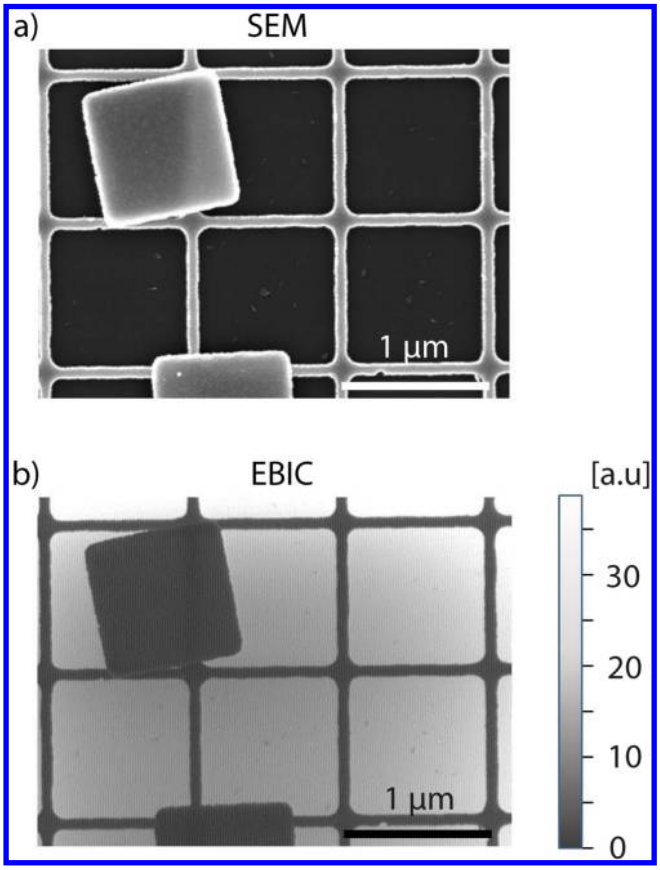

Figure 3. Electron-beam-induced current (EBIC) measurement of metal nanowire network MIS solar cell. (a) SEM image of a region of interest (ROI) of a similar sample to the one shown in Figure 2. Two residual metal flakes from the fabrication can be seen. (b) EBIC measurements, showing a uniform charge carrier separation and collection in the ROI due to the closely spaced metal nanowire network and the large carrier diffusion lengths in silicon. We note that the shadowed regions due to the metal nanowires are smaller for a sample under light illumination, because of efficient directional scattering by optical (plasmon) resonances.

DOI: 10.1021/acs.nanolett.6b00949
Nano Lett. 2016, 16, 3689−3695

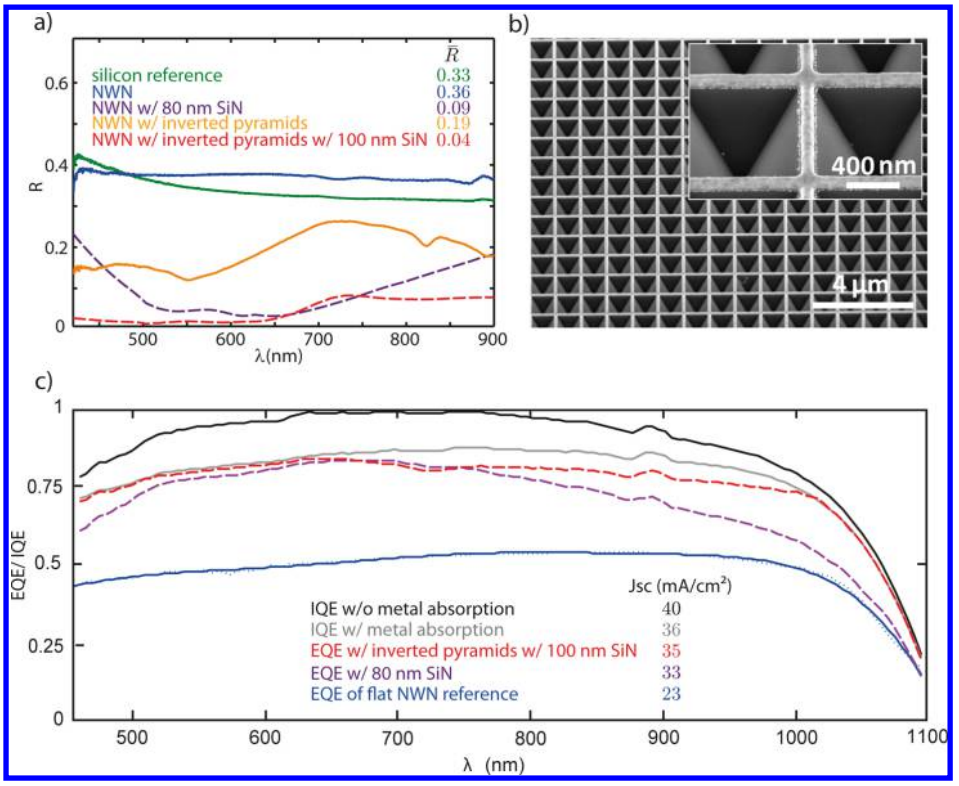

Figure 4. (a) Reflection measurements (solid lines) of silicon reference wafer (green), a solar cell with a metal nanowire network (NWN) with a pitch of 1 μm and a nanowire width of 100 nm (blue) and a sample with integrated inverted nanopyramids between the metal nanowires (orange). Also shown are the simulated reflection values (dashed lines) of the flat metal network with 80 nm SiN coating (violet) and the integrated inverted nanopyramid metal nanowire structure with 100 nm SiN coating (red). The average reflection values between 420−900 nm are listed next to the legend. (b) Scanning electron microscopy image of a metal nanowire network with integrated inverted nanopyramids. A high-resolution SEM is shown as an inset. (c) External quantum efficiency (EQE) of solar cell with metal nanowire network (blue). The IQE was determined by accounting for the reflection (blue line in (a)) and the simulated absorption of the metal network. The simulated reflection curves in (a) for the SiN coating (violet) and the integrated nanopyramid nanowire structure (red) were used to estimate the effect on the EQE of the final device. The respective short-circuit current densities are depicted next to the legend.

the V_{oc}, J_{sc}, and FF, are well below those of state of the art silicon solar cells. Therefore, we conduct the following electrical and optical analyses to get insight into the device performance and to point out crucial steps toward improvements.

Figures S6 and S7 show band diagram simulations that have been performed to study the dependence of the conduction type inversion, and hence selectivity of the MIS contact on the work function difference between the n-type silicon and the adjacent metal. The simulations show that high metal work functions (>5 eV) can lead to strong conduction type inversion in the underlying silicon, the prerequisite for a high V_{oc}. Conversely, any decrease of the effective metal WF will lead to a decrease in the V_{oc}. After considering other possibilities, we conclude that the cause for the relatively low V_{oc}, when compared to state-of-the-art silicon solar cells (>700 mV), can be the lowering of the Pd vacuum work function due to the presence of the dielectric Al_2O_3.[32] From developments in the field of complementary−metal−oxide−semiconductor (CMOS) transistors, it is known that Fermi level pinning to a charge neutrality level (CNL) in the dielectric can lower the effective work function of the metal.[32−34] Therefore, other dielectrics, for example, SiO_2, that cause much weaker Fermi level pinning to the CNL should be employed in future devices. However, when searching for alternatives the stability and passivation properties for ultrathin layers of 1−2 nm have to be kept in mind. For a detailed discussion see SI.

Besides the aforementioned reasons, the typically high costs associated with high WF metals (Ag, Au, Pd, Pt) and their potentially detrimental influence on the material quality (e.g., lifetime) have to be considered. Therefore, high WF oxides (e.g., MoOx) are a promising alternative as an interfacial layer.[35−37] The same holds for layers of doped semiconductors, like n-type (and p-type) a-Si:H in high-efficiency silicon heterojunction (SHJ) solar cells.[6,38] However, as also our results show (see Figure S10), the stability and process compatibility, especially with nanostructuring have to be considered when employing such layers.[39]

Besides the degree of conduction type inversion, the simulations also show that the depth of the inversion layer extends to about 200 nm into the silicon, depending on the metal work function. Given the nanowire network pitch of 1 μm and assuming a constant radial extend of the inversion around the metal as an upper bound, a large fraction of the silicon square between the metal wires is inverted close to the surface. Electron-beam-induced-current (EBIC) measurements (Figure 3) show that this conduction type inversion, together with the large diffusion lengths in silicon lead to a homogeneous charge carrier collection.

As can be seen in Figure 2, the J_{sc} of our solar cell reaches a value of 23 mA/cm^2. We ascribe the primary deviation from state-of-the-art silicon solar cells (~42 mA/cm^2) to the high reflectivity of the uncoated and flat silicon substrate. Therefore, we measure the total reflectance of the completed devices using

DOI: 10.1021/acs.nanolett.6b00949
Nano Lett. 2016, 16, 3689−3695

an integrating sphere setup. Then, we introduce a low reflectivity structure, consisting of nanopyramids integrated in between the nanowire network. We use EQE measurements to estimate the effect on the final device performance, as a first step toward improved J_{sc} values for nanostructures MIS solar cells.

Figure 4a shows the measured reflection values of the nanowire network solar cell from Figure 1 (blue), the network with integrated inverted nanopyramids (orange) and a bare polished silicon surface as reference (green). FDTD simulations were used to obtain an estimate of the residual reflection when a standard antireflection coating (n = 2) of 80 nm would be included on top of the flat nanowire network solar cell (violet). The average reflectivity ($\bar{R}$) in the wavelength range from 420−900 nm is also shown for the different structures. Figure 4c shows the measured external quantum efficiency (EQE, extracted charge carriers per incident photon) of the flat nanowire network solar cell (blue line). The curve shows relatively uniform quantum efficiency over the visible range. Taking into account the measured reflection and the simulated absorption in the metal, the internal quantum efficiency (IQE, extracted charge carriers per absorbed photon in the semiconductor) was determined (black line). For wavelengths below the band gap of silicon (1.1 eV), the IQE increases until it reaches unity in the range between 600−800 nm. For short wavelengths, the IQE drops to a value of ∼0.8, indicating charge carrier recombination near the front surface. The effect of detrimental absorption in the metal can be seen for the IQE with the metal absorption (gray line). To estimate the effect of a standard SiN AR coating on the optical response of the solar cell, the EQE was calculated taking into account the simulated reflection of Figure 4a (violet dashed line).

The measurements and simulations in Figure 4a show that the nanowire network only adds a small amount of additional reflection, the value increases from 33% for a bare silicon surface to 36%. For this sample we measured a J_{sc} of 23 mA/cm^2 (see Figure 2a and Figure 4c). A standard 80 nm AR coating (n = 2) can reduce the reflection of the flat nanowire network silicon surface to ∼9%, which would result in a short-circuit current density of ∼33 mA/cm^2 (see Figure 4c).

The measured J_{sc} of 23 mA/cm^2 (see Figure 2a) was obtained for a MIS solar cell with a bare nanowire network silicon surface with an average reflection of 36%. Therefore, the photocurrent density after subtracting the reflection losses amounts to 36 mA/cm^2 (gray curve in Figure 4c), which shows that a large fraction of the photogenerated charges is collected. However, because it does not reach the maximum photocurrent density under 1 sun illumination for silicon (∼44 mA/cm^2), we conclude that other loss mechanisms must be present, which are discussed below.

Figure S8 shows the simulated reflection, transmission, and absorption values for a metal nanowire network with the dimensions mentioned above on a flat silicon wafer. As can be seen, the averaged absorption amounts to ∼10% in the 420−900 nm spectral range. Therefore, we conclude, that the short-circuit current density is partly lowered due to absorption in the metal by approximately 4 mA/cm^2 to the value of 36 mA/cm^2 (black curve in Figure 4c). A potentially detrimental influence of the tunnel junction, which could result in nonlinear current−voltage behavior, was ruled out by measurements of the J_{sc} under different illumination intensities, which prove that the 1 nm Al_2O_3 has a negligible tunnel resistance under normal operation conditions (see Figure S9). Previous research has shown that the insulator thickness for MIS type solar cells should not exceed 2 nm to limit the tunnel resistance.[4,5]

Another origin of the photocurrent loss can be related to fabrication induced defect formation. After the fabrication of the metal nanowire networks, we encounter strongly s-shaped $I-V$ curves, which can be attributed to charge carrier extraction barriers at the contact-silicon interfaces.[40] We anneal our samples until the s-shape is completely removed. We ascribe the damage mostly to the electron beam exposure of the a-Si:H.[39] With increasing annealing temperatures, the I_{sc} (and FF) of the solar cells is monotonically increasing. However, the V_{oc} reaches its maximum at around 220−230 °C, after which it starts to decrease. Therefore, we chose the annealing temperature not to exceed 220 °C, recovering the maximum $V_{oc,}$ while being aware of the nonoptimized I_{sc} (and FF) values, due to residual fabrication induced defects. For further explanation, see the Figure S10. The IQE (black curve) in Figure 4c shows a decrease in IQE for short wavelength until it reaches ∼0.8. This supports our assumption as light in the short wavelengths range is absorbed close to the surface, where the fabrication induced defects must be located. Therefore, the annealing behavior and the absorption in the metal nanowire network discussed above can explain the main difference between the J_{sc} of our solar cells (36 mA/cm^2, after reflection) and a J_{sc} of 42 mA/cm^2, which is reached by highly efficient silicon solar cells. We note that other losses, such as parasitic absorption in the thin a-Si:H layer, are likely to be present.[41]

As a first step toward improved J_{sc} values for nanostructured MIS solar cells, we fabricate inverted nanopyramids integrated in between the metal nanowire network. Bare inverted nanopyramids with optimized pitch and additional AR coating have shown outstanding optical performance.[42,43]Furthermore, etch resistant metals, such as the ones employed for our metal nanowire network, are frequently used as masking layers in micro- and nanofabrication.[44,45] Figure 4b shows a scanning electron microscopy (SEM) image (magnified in the inset) of the fabricated inverted nanopyramid nanowire network structure. The measured reflection of the network with inverted pyramids (Figure 4a, solid yellow line) shows clear resonant features due to the diffraction modes created by the effective grating. The average reflectivity of 19% proves the strong decrease in reflection compared to the flat nanowire network surface. The simulated additional AR coating of 100 nm on top of the nanopyramid structure (Figure 4a, dashed red line) shows that the residual reflection can be even further reduced to 4%, which is well below the optimized AR coating for a flat silicon nanowire network surface (9%) (solid violet line). Figure 4c shows the effect of the integrated nanopyramid texturing on the EQE (red dashed curve), which results in a J_{sc} of ∼35 mA/cm^2. We stress that a further decrease in reflection with optimized dimensions, for example, AR coating thickness and wire thickness, can be expected. However, the optimization of the nontrivial optical response, as well as the integration into the solar cell fabrication process of the metal nanowire network with integrated nanopyramids is beyond the scope of this report and focus of ongoing research.

Conclusions. We successfully apply metal nanowire networks to the metal−insulator−semiconductor solar cell scheme. After correcting for the influence of the small size of the active area on the V_{oc} and the missing antireflection coating, our MIS solar cells exhibit a corrected power conversion efficiency of ∼11% with an effective V_{oc} of 560 mV and estimated J_{sc} of 33 mA/cm^2. We use EBIC measurements to show that the metal

DOI: 10.1021/acs.nanolett.6b00949
Nano Lett. 2016, 16, 3689−3695

nanowire network homogeneously extracts charge carriers via an inversion layer in the underlying silicon. Band diagram simulations allow us to investigate the dependence of the conduction type inversion on the work function difference between the metal and the semiconductor and indicate the occurrence of Fermi-level pinning at a charge neutrality level at the metal dielectric interface. Reflection measurements show that a high metal coverage of the surface with metal nanowire networks only adds 3% of additional reflection compared to a flat silicon surface. Finally, we demonstrate a first step toward improved device performance by using the metal nanowire network not only as a transparent electrode and for the inversion layer formation, but also as an etch mask for surface texturing. We fabricate inverted nanopyramids integrated into the metal nanowire network. This way we are able to decrease the reflectivity substantially from 36% to ∼4%. We use EQE measurements to estimate the influence of the reduced reflection on the overall device performance and thereby point out a path toward MIS solar cells that exhibit both high V_{oc} and J_{sc} values. Furthermore, our work shows potential for the MIS concept to be used to directly contact well passivated, intrinsic semiconducting layers, which naturally show higher carrier lifetimes and mobilities and are therefore preferable for high efficiency solar cells. Finally, our results are not limited to silicon, but can be applied to many thin-film materials with small charge carrier diffusion lengths where the difficulty of doping makes carrier selective contact formation more challenging.

■ ASSOCIATED CONTENT

Supporting Information

The Supporting Information is available free of charge on the ACS Publications website at DOI: 10.1021/acs.nanolett.6b00949.

Details of device fabrication, electrical and optical characterization and optical simulations, masked measurements and the influence of a small active area fabricated on a large substrate, scaling behavior of J_0 with area size, variation of the V_{oc} for masked and unmasked measurements at 1 sun; band diagram simulations, influence of fixed charge density of Al_2O_3 on extent of inversion layer; optical FDTD simulations of metal nanowire network, tunnel resistance, investigation of annealing behavior. (PDF)

■ AUTHOR INFORMATION

Corresponding Author

*E-mail: garnett@amolf.nl.

Notes

The authors declare no competing financial interest.

■ ACKNOWLEDGMENTS

We are thankful to S. Mann for the EQE measurements and for the useful discussions with B. Ehrler, M. Knight, and W. C. Sinke. This work is part of the research program of the Foundation for Fundamental Research on Matter (FOM), which is part of The Netherlands Organization for Scientific Research (NWO). The research leading to these results has received funding from the European Research Council under the European Union's Seventh Framework Programme (FP/2007-2013)/ERC Grant 337328 "NanoEnabledPV" and ERC Grant 267634 "Plasmeta". Furthermore, we would like to acknowledge the funding from the NanoNextNL program, a technology program (project 2A.01) of the Dutch Ministry of Economic Affairs."

■ REFERENCES

(1) Sze, S. M.; Ng, K. K. *Physics of Semiconductor Devices*, 3rd ed.; Wiley: NJ, 2007.
(2) Godfrey, R. B.; Green, M. A. *Appl. Phys. Lett.* **1979**, *34*, 790−793.
(3) Hezel, R. *Prog. Photovoltaics* **1997**, *5*, 109−120.
(4) Green, M. A.; King, F. D.; Shewchun, J. *Solid-State Electron.* **1974**, *17*, 551−561.
(5) Shewchun, J.; Green, M. A.; King, F. D. *Solid-State Electron.* **1974**, *17*, 563−572.
(6) Feldmann, F.; Bivour, M.; Reichel, C.; Hermle, M.; Glunz, S. W. *Proceedings of the 28th Eur. Photovolt. Sol. Energy Conf. Exhib.*, Paris, France, 2013; pp 988−992.
(7) Feldmann, F.; Simon, M.; Bivour, M.; Reichel, C.; Hermle, M.; Glunz, S. W. *Appl. Phys. Lett.* **2014**, *104*, 181105.
(8) Glunz, S. W.; Feldmann, F.; Richter, A.; Bivour, M.; Reichel, C.; Steinkemper, H.; Benick, J.; Hermle, M. *Proceedings of the 31st Eur. Photovolt. Sol. Energy Conf. Exhib.*, Hamburg, Germany, 2015; pp 259−263.
(9) Scheuermann, A. G.; Lawrence, J. P.; Kemp, K. W.; Ito, T.; Walsh, A.; Chidsey, C. E. D.; Hurley, P. K.; McIntyre, P. C. *Nat. Mater.* **2015**, *15*, 99.
(10) Chen, Y. W.; Prange, J. D.; Dühnen, S.; Park, Y.; Gunji, M.; Chidsey, C. E. D.; McIntyre, P. C. *Nat. Mater.* **2011**, *10*, 539−544.
(11) Esposito, D. V.; Levin, I.; Moffat, T. P.; Talin, a A. *Nat. Mater.* **2013**, *12*, 562−568.
(12) Hill, J. C.; Landers, A. T.; Switzer, J. A. *Nat. Mater.* **2015**, *14*, 1150.
(13) Hezel, R.; Meyer, R.; Metz, A. *Sol. Energy Mater. Sol. Cells* **2001**, *65*, 311−316.
(14) Van de Groep, J.; Spinelli, P.; Polman, A. *Nano Lett.* **2012**, *12*, 3138−3144.
(15) Catrysse, P. B.; Fan, S. *Nano Lett.* **2010**, *10*, 2944−2949.
(16) Kuang, P.; Park, J.-M.; Leung, W.; Mahadevapuram, R. C.; Nalwa, K. S.; Kim, T.-G.; Chaudhary, S.; Ho, K.-M.; Constant, K. *Adv. Mater.* **2011**, *23*, 2469−2473.
(17) De, S.; Higgins, T. M.; Lyons, P. E.; Doherty, E. M.; Nirmalraj, P. N.; Blau, W. J.; Boland, J. J.; Coleman, J. N. *ACS Nano* **2009**, *3*, 1767−1774.
(18) Ye, S.; Rathmell, A. R.; Chen, Z.; Stewart, I. E.; Wiley, B. J. *Adv. Mater.* **2014**, *26*, 6670−6687.
(19) Song, T.-B.; Seung Rim, Y.; Liu, F.; Bob, B.; Ye, S.; Hsieh, Y.-T.; Yang, Y. *ACS Appl. Mater. Interfaces* **2015**, *7*, 24601−24607.
(20) Gaynor, W.; Lee, J.-Y.; Peumans, P. *ACS Nano* **2010**, *4*, 30−34.
(21) Yang, L.; Zhang, T.; Zhou, H.; Price, S. C.; Wiley, B. J.; You, W. *ACS Appl. Mater. Interfaces* **2011**, *3*, 4075−4084.
(22) Garnett, E. C.; Cai, W.; Cha, J. J.; Mahmood, F.; Connor, S. T.; Greyson Christoforo, M.; Cui, Y.; McGehee, M. D.; Brongersma, M. L. *Nat. Mater.* **2012**, *11*, 241−249.
(23) Lee, J. Y.; Connor, S. T.; Cui, Y.; Peumans, P. *Nano Lett.* **2008**, *8*, 689−692.
(24) Van de Groep, J.; Gupta, D.; Verschuuren, M. a.; Wienk, M. M.; Janssen, R. a. J.; Polman, A. *Sci. Rep.* **2015**, *5*, 11414.
(25) Smit, S.; Garcia-Alonso, D.; Bordihn, S.; Hanssen, M. S.; Kessels, W. M. M. *Sol. Energy Mater. Sol. Cells* **2014**, *120*, 376−382.
(26) Dingemans, G.; Seguin, R.; Engelhart, P.; van den Sanden, M. C. M.; Kessels, W. M. M. *Phys. Status Solidi RRL* **2010**, *1−2*, 10−12.
(27) Hoex, B.; Gielis, J. J. H.; van de Sanden, M. C. M.; Kessels, W. M. M. *J. Appl. Phys.* **2008**, *104*, 113703.
(28) Hoex, B.; Schmidt, J.; Bock, R.; Altermatt, P. P.; van de Sanden, M. C. M.; Kessels, W. M. M. *Appl. Phys. Lett.* **2007**, *91*, 112107.
(29) Benick, J.; Hoex, B.; van de Sanden, M. C. M.; Kessels, W. M. M.; Schultz, O.; Glunz, S. W. *Appl. Phys. Lett.* **2008**, *92*, 253504.
(30) Dingemans, G.; Kessels, W. M. M. *J. Vac. Sci. Technol., A* **2012**, *30*, 040802.

DOI: 10.1021/acs.nanolett.6b00949
Nano Lett. 2016, 16, 3689−3695

(31) Brittman, S.; Adhyaksa, G. W. P.; Garnett, E. C. *MRS Commun.* **2015**, *5*, 7−26.
(32) Yeo, Y. C.; King, T. J.; Hu, C. *J. Appl. Phys.* **2002**, *92*, 7266−7271.
(33) Tersoff, J. *Phys. Rev. Lett.* **1984**, *52*, 465−468.
(34) Prada, S.; Martinez, U.; Pacchioni, G. *Phys. Rev. B: Condens. Matter Mater. Phys.* **2008**, *78*, 1−8.
(35) Bullock, J.; Hettick, M.; Geissbühler, J.; Ong, A. J.; Allen, T.; Sutter-Fella, C. M.; Chen, T.; Ota, H.; Schaler, E. W.; De Wolf, S.; Ballif, C.; Cuevas, A.; Javey, A. *Nat. Energy* **2016**, *1*, 15031.
(36) Battaglia, C.; De Nicolás, S. M.; De Wolf, S.; Yin, X.; Zheng, M.; Ballif, C.; Javey, A. *Appl. Phys. Lett.* **2014**, *104*, 1113902.
(37) Geissbühler, J.; Werner, J.; Martin de Nicolas, S.; Barraud, L.; Hessler-Wyser, A.; Despeisse, M.; Nicolay, S.; Tomasi, A.; Niesen, B.; De Wolf, S.; Ballif, C. *Appl. Phys. Lett.* **2015**, *107*, 081601.
(38) Mishima, T.; Taguchi, M.; Sakata, H.; Maruyama, E. *Sol. Energy Mater. Sol. Cells* **2011**, *95*, 18−21.
(39) Schade, H.; Pankove, J. *J. Phys. Colloq.* **1981**, *42*, 327−330.
(40) Wagenpfahl, A.; Rauh, D.; Binder, M.; Deibel, C.; Dyakonov, V. *Phys. Rev. B: Condens. Matter Mater. Phys.* **2010**, *82*, 115306.
(41) Holman, Z. C.; Descoeudres, A.; Barraud, L.; Fernandez, F. Z.; Seif, J. P.; De Wolf, S.; Ballif, C. *IEEE J. Photovoltaics* **2012**, *2*, 7−15.
(42) Mavrokefalos, A.; Han, S. E.; Yerci, S.; Branham, M. S.; Chen, G. *Nano Lett.* **2012**, *12*, 2792−2796.
(43) Han, S. E.; Chen, G. *Nano Lett.* **2010**, *10*, 4692−4696.
(44) Lim, K. M.; Gupta, S.; Ropp, C.; Waks, E. *Microelectron. Eng.* **2011**, *88*, 994−998.
(45) Franssila, S. *Introduction to Microfabrication*, 2nd ed.; Wiley: Chichester, 2010.

DOI: 10.1021/acs.nanolett.6b00949
Nano Lett. 2016, 16, 3689−3695